Dynamics of double emulsion break-up in three phase glass capillary microfluidic devices
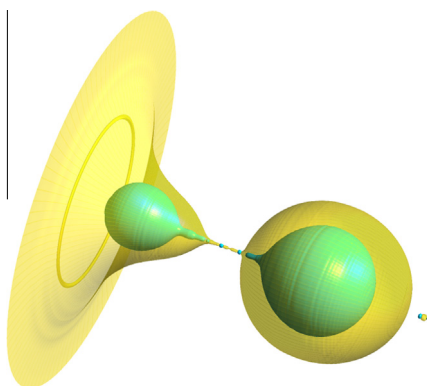
CrossMark

Seyed Ali Nabavi [a], Sai Gu [a,*], Goran T. Vladisavljević [b,*], Ekanem E. Ekanem [b]

[a] Offshore, Process and Energy Engineering Department, Cranfield University, Cranfield MK43 0AL, United Kingdom
[b] Department of Chemical Engineering, Loughborough University, Loughborough LE11 3TU, United Kingdom

GRAPHICAL ABSTRACT

ARTICLE INFO

ABSTRACT

Pinch-off of a compound jet in 3D glass capillary microfluidic device, which combines co-flowing and countercurrent flow focusing geometries, was investigated using an incompressible three-phase axisymmetric Volume of Fluid–Continuum Surface Force (VOF–CSF) numerical model. The model showed good agreement with the experimental drop generation and was capable of predicting formation of core/shell droplets in dripping, narrowing jetting and widening jetting regimes. In dripping and widening jetting regimes, the presence of a vortex flow around the upstream end of the necking thread facilitates the jet break-up. No vortex flow was observed in narrowing jetting regime and pinch-off occurred due to higher velocity at the downstream end of the coaxial thread compared to that at the upstream end. In all regimes, the inner jet ruptured before the outer jet, preventing a leakage of the inner drop into the outer fluid. The necking region moves at the maximum speed in the narrowing jetting regime, due to the highest level of shear at the outer surface of the thread. However, in widening jetting regime, the neck travels the longest distance downstream before it breaks.

1. Introduction

Engulfment of core material within an insoluble shell and formation of core/shell microcapsules has attracted a lot of interest due to the ability of shell to act as a temporal or permanent barrier

* Corresponding authors at: School of Engineering, Cranfield University, United Kingdom. Fax: +44 1234 754685 (S. Gu). Fax: +44 1509223923 (G.T. Vladisavljević).
   E-mail addresses: s.gu@cranfield.ac.uk (S. Gu), g.vladisavljevic@lboro.ac.uk (G.T. Vladisavljević).

and protective layer for the core material [1]. Typical applications of core–shell capsules include protection of sensitive food ingredients from the environment [2], controlled drug delivery [3,4], and encapsulation of living cells [5] and solvents [6]. Conventional methods for the production of core–shell capsules are complex coacervation [7], internal phase separation [8], layer-by-layer electrostatic deposition [9], interfacial polymerisation [10], and spray drying [11]. However, the current methods usually require multi-stage processing and specific product formulation and allow limited control over the capsule size.

A precise control over the droplet morphology can be achieved using microfluidic emulsification strategies such as flow focusing [12], T-junction [13], and co-flowing [14]. One of the promising type of microfluidic devices is a 3D glass capillary microfluidic device developed by Utada et al. [15] by combining a co-flowing and flow focusing device. Flow focusing in a 3D glass capillary device is a useful strategy to minimise wetting problems found in planar PDMS co-flow-focusing devices [16]. Double emulsion droplets in microfluidic devices can be formed in three distinct regimes: dripping, narrowing jetting and widening jetting [15], whose transitions are affected by the interactions between interfacial, viscous, and inertial forces [17]. In the dripping regime, where fluid flow rates are low, interfacial tension dominates over inertial and viscous forces and droplets are produced close to the injection channel [18]. Narrowing jetting occurs when the viscous force caused by high velocity of the continuous phase exceeds the interfacial force, resulting in a long thinning jet that breaks up into small droplets far from the injection channel. In widening jetting, the dripping to jetting transition is caused by high velocity of the dispersed phase. When the inertial force of dispersed phase exceeds the interfacial tension, a fast widening jet is formed which breaks up into large droplets. The outer fluid exerts a drag force on the dispersed phase, leading to deceleration of the jet and its widening shape.

The previous studies on formation of double emulsions in microfluidic devices have dealt with the effects of fluid flow rates, fluid properties and device geometry on droplet size and dripping-to-jetting transition [15,19–26]. A study of the jet break-up mechanisms during microfluidic formation of double emulsions is largely missing. Velocity field and pressure distributions are of vital importance for studying the droplet break-up in microfluidic channels, but they are not easy to measure because of the small time and length scales. Velocity fields in microfluidic devices can be measured experimentally using micro-scale Particle Image Velocimetry (μPIV) [27], but the method is time consuming, costly and sometimes lead to low-quality images [28]. Due to limitations of the experimental methods, fundamental studies of microfluidic droplet formation are mainly based on numerical models or analytical solutions. A very limited number of numerical and analytical studies of droplet break-up in microfluidic systems have been done [24,29–33], dealing with single emulsions [30] or often limited to temporal evolution of interface and very narrow domain of drop formation [31–34]. Vu et al. [24] studied double emulsion formation in dripping regimes using flow vectors and reported the presence of a circulating flow around both interfaces. However, they have not covered drop generation in widening and narrowing jetting regimes, which are driven by distinct forces.

This work aims to provide in-depth analysis of the break-up of coaxial jets of immiscible liquids within a 3D glass capillary device in three distinct formation regimes, based on pressure and velocity fields simulated using a VOF–CSF numerical model. The VOF–CSF method has shown a good capability in predicting droplet formation in various microfluidic geometries [16,30,35–37], but it has never been used to simulate droplet formation in three-liquid phase 3D microfluidic devices [15]. The results can be used to improve the current understanding of hydrodynamic flow focusing in multi-liquid phase microfluidic systems and discover the physics underlying pinch-off of double emulsion droplets in dripping, narrowing jetting and widening jetting regimes.

2. Governing equations and numerical method

2.1. Governing equations

A two-dimensional incompressible axisymmetric VOF–CSF (Volume of Fluid–Continuum Surface Force) [38,39] numerical model has been developed in order to simulate double emulsion formation in a three phase glass capillary microfluidic device. The governing equations are those of mass, Eq. (1), and momentum equations, Eq. (2):

$$\frac{\partial \rho}{\partial t} + \frac{\partial (\rho U_i)}{\partial x_i} = 0 \qquad (1)$$

$$\frac{\partial (\rho U_i)}{\partial t} + \frac{\partial (\rho U_i U_j)}{\partial x_j} = -\frac{\partial P_i}{\partial x_i} + \frac{\partial}{\partial x_j}\left(\mu \frac{\partial U_i}{\partial x_j}\right) + F_i \qquad (2)$$

where U and P are velocity and pressure respectively, t, μ and ρ are time, dynamic viscosity and density, and F_i is a source term which includes interfacial force, F_γ and gravitational force. Since the characteristic length (e.g. diameter) is in the order of micrometre, the gravitational force can be neglected and $F_i = F_\gamma$. In the VOF approach, a momentum equation is solved for all the phases and the advection of interface is calculated by solving Eq. (3) for volume fraction, f:

$$\frac{\partial f}{\partial t} + \frac{\partial (U_i f)}{\partial x_i} = 0 \qquad (3)$$

The volume fraction determines the portion of the cell which is filled with either phase. Eqs. (4) and (5) are used to calculate ρ and μ in mass and momentum equations:

$$\mu = f\mu_1 + (1-f)\mu_2 \qquad (4)$$

$$\rho = f\rho_1 + (1-f)\rho_2 \qquad (5)$$

where subscripts 1 and 2 refer to phase 1 and 2 existing within the cell. CSF method [39] was used to calculate F_γ as follows:

$$F_\gamma = \sigma \kappa \nabla f \qquad (6)$$

where κ and γ are the local curvature of the interface and the interfacial tension respectively. κ is calculated as follows:

$$\kappa = \nabla \cdot \hat{n} \qquad (7)$$

and $\hat{n}$ is the unit normal vector defined as:

$$\hat{n} = \frac{\nabla f}{|\nabla f|} \qquad (8)$$

2.2. Numerical method

The governing equations were discretised using a transient pressure-based segregated algorithm in a finite-volume based commercial software Ansys® Fluent v. 14.0. A second order upwind scheme was used to approximate the discretised moment equation. It should be mentioned that the QUICK scheme was used as well. However, since there was no discrepancy between the solutions of the two approaches, second order upwind scheme, which was computationally less expensive, was selected to carry out the simulations. PRESTO scheme was used to calculate the exact value of pressure on the cell faces in order to prevent the interpolation errors. The pressure–velocity coupling was accomplished by SIMPLE scheme and the interpolation of interface was achieved by Geo-Reconstruct algorithm. A variable time step method

defined by Courant number, Co (a non-dimensional number which gives a comparison between the time step and transit characterisation time that a fluid element covers within a control volume) was used in order to reduce the computational cost and facilitate the numerical model convergence. In the current simulations, Co is 0.35. A high-resolution mesh is required since the shell thickness during droplet elongation can be only 10 μm and at least three mesh elements are required across the shell to simulate the drop formation successfully. Under such circumstances, a three-dimensional numerical model would require a very large computational source. Therefore, a two-dimensional axisymmetric CFD model was developed.

The grid dependency was carried out by producing five meshes with resolutions of 8, 4, 3, 2, and 1 μm based on developing the compound jet through the collection tube, where the solutions achieved in the mesh with resolution of 3–1 μm were similar. In order to achieve a high accuracy of simulations at reasonable computational costs, a very fine mesh of 3 μm was used around the injection nozzle and collection tube where the droplets are formed, while a much coarser mesh was used in the rest of the domain. A schematic of computational domain and the generated mesh is given in Supplementary Material A (Fig. sA.1). Since the CFD model is axisymmetric, the reproduced results are based on three-dimensional solutions. Table 1 provides a summary of the boundary conditions used.

3. Experimental verification

Capillary microfluidic devices are coaxial assemblies of round and square glass capillaries attached onto a microscope slide. A detailed description of the device fabrication and the materials used for emulsion formation is provided in Supplementary Material A. The liquids were delivered to the device via polyethylene medical tubing (0.86 mm I.D. and 1.52 mm O.D.) from gas-tight glass

Table 1
Summaries of boundary conditions.

Boundary	Type
Inlets	Mass flow inlet
Outlet	Pressure outlet
Symmetry axis	Axis
Wall	No-slip wall

syringes mounted on separate Harvard Apparatus model 11 Elite syringe pumps. Emulsion droplets were formed at the entrance of the collection capillary as a result of the break-up of coaxial jet composed of inner and middle fluid (Fig. 1). The droplet formation was monitored using an inverted microscope (XDS-3, GX Microscopes, UK) and Phantom V9.0 high-speed camera interfaced to a PC computer. Fig. 1 shows a schematic of experimental setup.

Fig. 2 provides a qualitative experimental validation of the numerical model. It can be seen that the CFD model successfully predicts morphological changes of both interfaces during double emulsion formation. At $t = 0$, the compound jet contains one detached inner droplet and a new droplet grows at the injection nozzle. At $t = 1.67$ ms, the compound jet contains two inner droplets and has a maximum length, which is 4 times greater than the diameter D_{Orif} of the orifice in the collection capillary. At $t = 3.67$ ms, the middle phase jet has just ruptured and a narrow filament of middle fluid is still visible between the detached double emulsion droplet and the ruptured jet. Although the CFD model is able to accurately predict the hydrodynamic behaviour, it does not
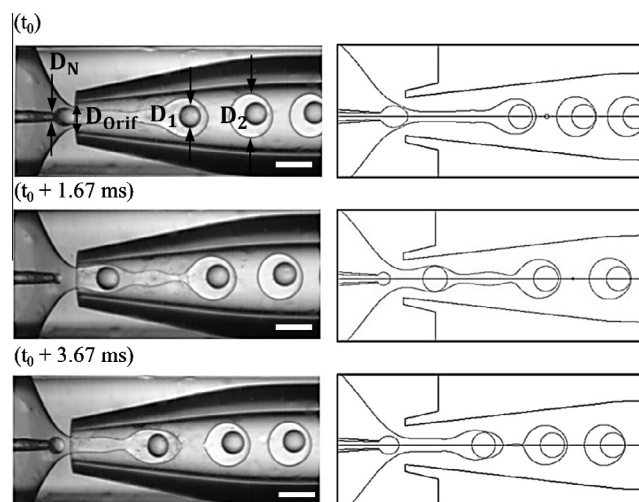

Fig. 2. A comparison of droplet formation behaviour in dripping regime using experimental (left) and numerical (right) images. D_1 and D_2 is the diameter of inner and outer droplet, respectively and D_N is the diameter of the injection nozzle. The scale bars are 300 μm. Movie 2.
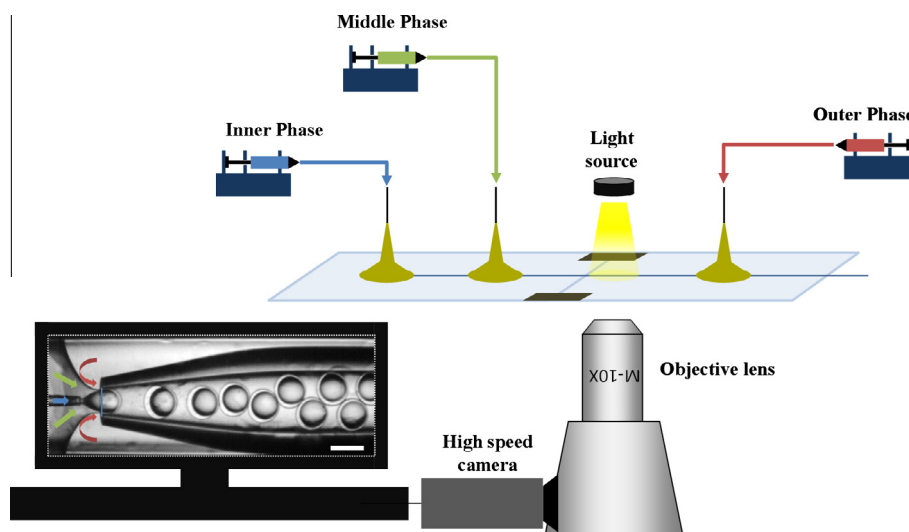

Fig. 1. A schematic view of the experimental setup used in this work. The direction of flow of inner, middle and outer fluid is shown by blue, green and red arrow, respectively. The scale bars are 300 μm. Movie 1. (For interpretation of the references to colour in this figure legend, the reader is referred to the web version of this article.)
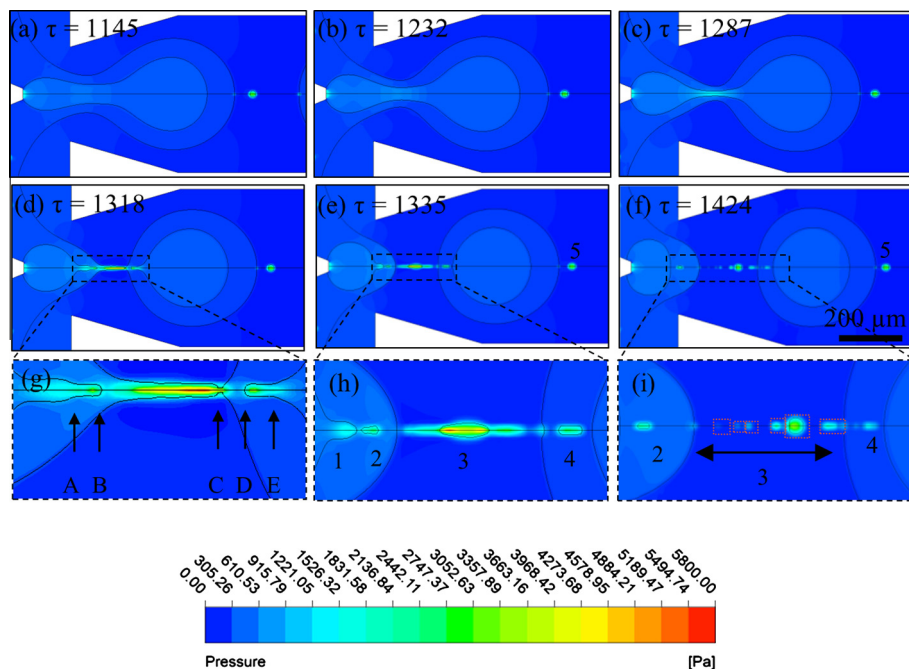
Fig. 3. (a)–(f). Image sequences of droplet pinch off in dripping regime based on pressure distribution contours. $Q_1 = 0.37$ ml/h, $Q_2 = 0.92$ ml/h, $Q_3 = 2.47$ ml/h, $\rho_1 = 1180$ kg/m³, $\rho_2 = 1170$ kg/m³, $\rho_3 = 1200$ kg/m³, $\mu_1 = 0.0396$ Pa s, $\mu_2 = 0.0648$ Pa s, $\mu_3 = 0.0482$ Pa s, $\sigma_{12} = 0.00574$ N/m, $\sigma_{23} = 0.0137$ N/m, $D_N = 25$ μm, $D_{Orif} = 300$ μm. $D_2 = 379$ μm, $D_1 = 247.5$ μm, $\tau_2 = 1324$, $t_2 = 77.4$ ms. (g)–(i) are magnified images of the dashed boxes shown in (d)–(f), respectively.

account for the adsorption of surfactant molecules at the interfaces and droplet repulsion by steric or electrostatic effects. Therefore, coalescence of inner droplets was observed, as shown in Fig. 5f.

4. Results and discussion

The break-up mechanisms of double emulsion droplets in three-phase capillary devices has not yet been fully investigated due to the presence of two interfaces and 3D geometry, which complicates the underlying physics. The physical properties of fluids used in simulations will correspond to encapsulation of 30 wt% aqueous monoethanolamine (MEA) solution within a UV-curing Norland Optical Adhesive 61 (NOA 61) liquid [6]. The break up mechanisms of double emulsion within a glass capillary microfluidic device in dripping, widening jetting and narrowing jetting regime (Fig. sA.2) will be discussed in the following sections.

4.1. Dripping regime

Image sequences of droplet pinch-off in dripping regime are given in Figs. 3 and 4. Zero time ($\tau = 0$) corresponds to the beginning of droplet growth, where $\tau = V_{1,N}t/R_N$ is a non-dimensional time, $V_{1,N}$ is the average velocity of dispersed phase at the injection nozzle, t is a real time, and R_N is the radius of injection nozzle. The breakup of inner and outer filament takes place at $\tau_1 = 1309$ and $\tau_2 = 1324$, respectively. The compound jet starts to pinch-off with enlarging and stretching of the double emulsion droplet, which results in the appearance of a neck between the jet and the growing droplet (Fig. 3b). Further elongation of the droplet caused by the growing drag force, which is proportional to the droplet diameter, leads to thinning of the neck. A high pressure region in the middle of the neck accelerates narrowing of a coaxial thread of inner and middle fluid by pushing both fluids to either side of the neck, where the pressure is lower (Fig. 3c). Due to collision of the fluid streams from opposite directions within the jet, a vortex

flow is formed in a dashed box region in Fig. 4c. The reversed flow tends to pull back the jet, which eventually ruptures the inner filament and forms the inner droplet. Fig. 4g is a magnified view of the dashed box in Fig. 4c, showing vortices in the inner and middle fluid. Finally, the vortex flow extends to the outer fluid, which results in the breakup of the middle phase thread. Fig. 4h is a magnified image of the dashed box in Fig. 4d, showing a vortex flow in the outer fluid around the upstream end of the middle fluid thread shortly after collapse of the inner fluid filament.

Fig. 3g shows a thin neck formed at the downstream end of the middle phase thread at $\tau = 1318$. Once the neck collapses, the elongated filament of the middle phase with a diameter of 5.6 μm rapidly retreats to the remaining compound jet due to imbalance in capillary pressure. Meanwhile, the presence of vortex flow at the remaining cone-shaped jet and the tendency of the outer interface to become spherical due to interfacial tension, leads to breakup of the middle phase thread at its upstream end and formation of primary satellite droplet at $\tau = 1331$. Fig. 3h shows such satellite droplet (in region 3) at $\tau = 1335$, i.e. 0.4 ms after it has been formed.

Fig. 3g–i explains formation of satellites and sub-satellites during pinch-off. Fig. 3g is a magnified view of the elongated thread of middle fluid between two inner droplets just before its break-up. The break-up region can be divided into three zones: A–B, which is a narrow tip left behind the breakup of inner fluid filament; B–C is the middle fluid thread attached to the shell of the subsequent double emulsion droplet through neck C, and D–E, which is an inner fluid filament connected to the detached inner droplet. Fig. 4h and i are magnified views of the break-up region after complete rupture of the compound thread. Satellite droplet 2 in Fig. 3h is formed by the breakup of the inner filament (A–B) and 1 is a residue of the inner filament after breakup. Due to strong vortex flow, filament 1 will retract to the middle fluid, suppressing further formation of satellite droplets at that location. Satellite droplet 2 will eventually coalescence with a neighbouring core droplet at $\tau = 1557$, i.e. 13.7 ms after its formation. Segment B–C of the middle fluid undergoes multiple pinch-offs, resulting in the formation
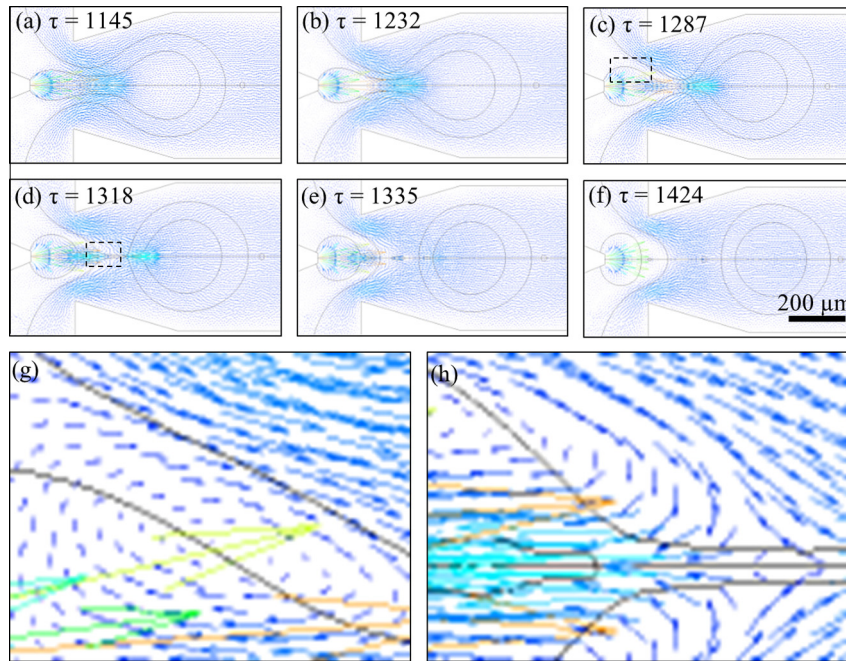
Fig. 4. (a)–(f) Sequences of images depicting the pinch off in dripping regime based on velocity vector profile. (g) Magnified image of the boxed region in (c) showing vortex flow in the inner and middle fluid; (h) magnified image of the boxed region in (d) showing vortex flow in the outer fluid. The conditions are the same as in Fig. 3.
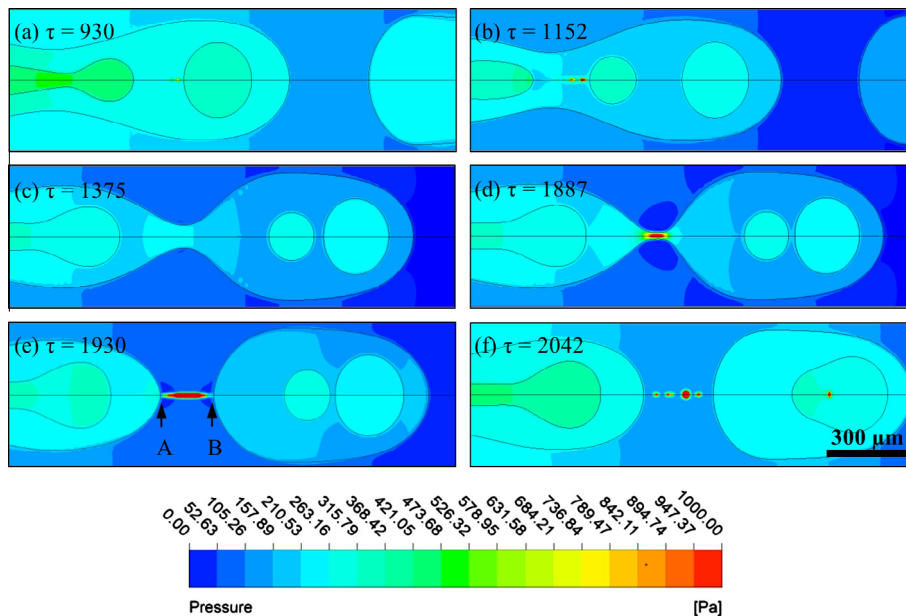

Fig. 5. Image sequences of droplet pinch off in widening jetting regime based on pressure distribution contours. $Q_1 = 0.37$ ml/h, $Q_2 = 2.31$ ml/h, $Q_3 = 2.47$ ml/h, $\rho_1 = 1180$ kg/m³, $\rho_2 = 1170$ kg/m³, $\rho_3 = 1200$ kg/m³, $\mu_1 = 0.0396$ Pa s, $\mu_2 = 0.0648$ Pa s, $\mu_3 = 0.0482$ Pa s, $\sigma_{12} = 0.00574$ N/m, $\sigma_{23} = 0.0137$ N/m, $D_N = 25$ μm, $D_{Orif} = 300$ μm, $D_2 = 589.8$ μm, $D_1 = 164.5$ μm, $\tau_2 = 1900$, $t_2 = 111.1$ ms.

of six satellite droplets of different sizes in the region 3 in Fig. 3i. Another relatively large inner satellite droplet will be formed by the break-up of filament D–E and the location of this satellite droplet is denoted by 4 in Fig. 4h and i. The satellite droplet 4 will coalescence with a neighbouring core droplet at $\tau = 1424$, i.e. 5.9 ms after its formation.

4.2. Widening jetting regime

A series of images depicting a breakup of double emulsion droplet in widening jetting is shown in Figs. 5 and 6. The transition

from dripping to widening jetting was achieved by increasing Q_2 from 0.92 to 2.31 ml/h while keeping constant all other parameters in Figs. 4 and 5. The jet breakup is induced by a high middle fluid velocity, which surpasses the outer fluid velocity. The breakup of the core primary droplet occurs at $\tau_1 = 1046$, which is almost 50 ms earlier than the breakup of the shell fluid, which occurs at $\tau_2 = 1900$. A long time between the two breakup events was due to the high shear force on the inner interface exerted by the middle fluid leading to fast detachment of inner droplets. As can be seen in Fig. 5b, when an inner droplet breaks-off from a thinning thread, two inner satellite droplets are formed behind the main droplet,
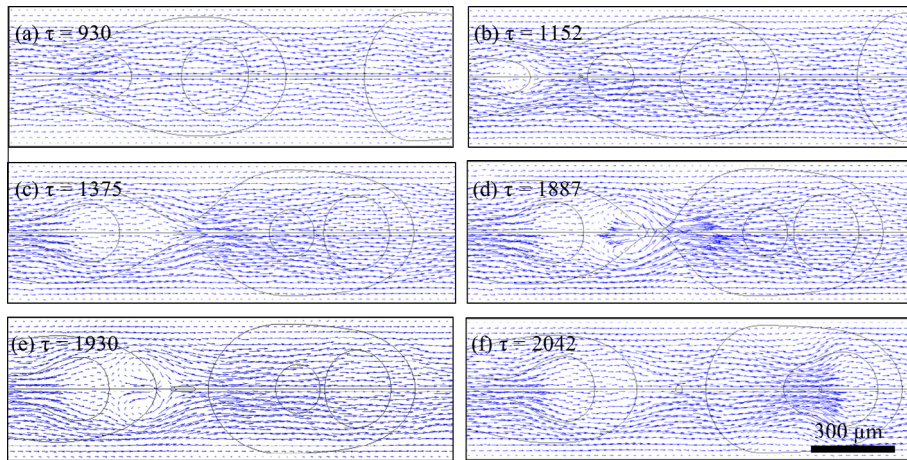
Fig. 6. Sequences of images depicting the pinch off in widening jetting regime based on velocity vector profile. The conditions are the same as in Fig. 5.
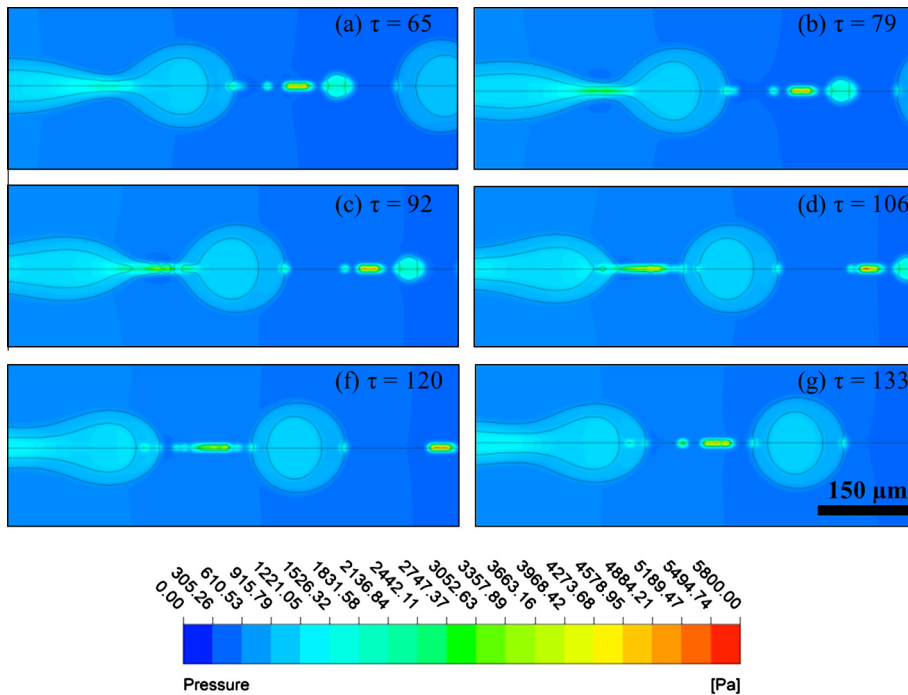

Fig. 7. Image sequences of droplet pinch-off in narrowing jetting regime based on pressure distribution contours. $Q_1 = 0.37$ ml/h, $Q_2 = 0.92$ ml/h, $Q_3 = 24$ ml/h, $\rho_1 = 1180$ kg/m^3, $\rho_2 = 1170$ kg/m^3, $\rho_3 = 1200$ kg/m^3, $\mu_1 = 0.0396$ Pa s, $\mu_3 = 0.0482$ Pa s, $\sigma_{12} = 0.00574$ N/m, $\sigma_{23} = 0.0137$ N/m, $D_N = 25$ μm, $D_{Orif} = 300$ μm. $D_2 = 160$ μm, $D_1 = 103$ μm, $\tau_2 = 111$, $t_2 = 5.2$ ms.

but they disappear at $\tau = 1226$ due to coalescence with the main droplet. Once the neck appears, a strong vortex flow is formed upstream of the thread due to collision of two oppositely directed streams of the middle fluid: the one sent by the pump to the neck in the downstream direction and another one in the upstream direction driven by high capillary pressure in the neck. The presence of reversed flow at the entrance of the neck (Fig. 6d) tends to pull back the neck. At the downstream end of the neck the created vortex tends to increase the velocity of the middle fluid and push forward the detaching double emulsion droplet. Since the neck is pulled in opposite directions, it collapses at both ends, which leads to the formation of a compound drop and a satellite droplet. The vortex flow at the front of the jet is still present at $\tau = 1930$ (Fig. 6e), i.e. shortly after the outer droplet pinches off. The subsequent inner droplet is pushed back by the vortex and does not grow until the vortex completely disappears. At

$\tau = 2042$ (Fig. 6f), the vortex is fully suppressed and droplet can start to grow. The middle fluid thread pinches off at both ends almost simultaneously with a delay between the two pinch-off events of just 0.2 ms, which is negligible compared to the total droplet formation time of $t_2 = 1899.4$ ms.

The velocity of the middle fluid at the upstream and downstream end of the thread (points A and B in Fig. 5e) at the moment of pinch-off is very similar, $V_A = 0.24V_{1,N}$ and $V_B = 0.25V_{1,N}$. After detachment, the primary satellite droplet exhibits multiple pinch-offs resulting in four satellite droplets shown in Fig. 5e. However, because of the significant difference in size between satellite and primary droplets, a high pressure difference is created which rapidly drives the satellite droplets towards the primary drop, which eventually results in fusion of the satellite droplets with the primary droplet at $\tau = 2742$. In addition, the pressure at the middle of the thread at the moment of pinch-off (Fig. 5d) is
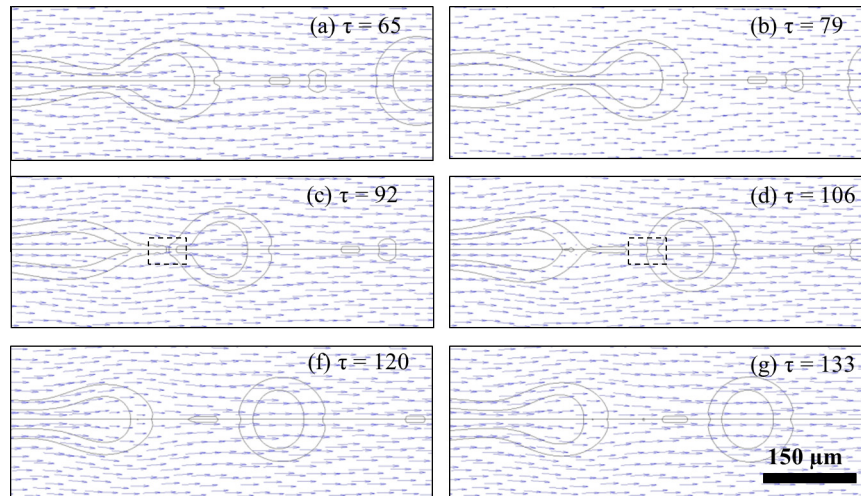
Fig. 8. Image sequences of droplet pinch-off in narrowing jetting regime based on velocity vector profile. The conditions are the same as in Fig. 7.

Table 2
Properties of phases used for emulsion preparation.

Phase	Density (kg/m^3)	Viscosity (Pa s)
Inner phase (1)	1012	0.00124
Middle phase (2)	940	0.01037
Outer phase (3)	1107	0.007912

considerably lower than that in dripping and narrowing jetting regime (Figs. 3d and 7c).

4.3. Narrowing jetting regime

Sequences of images describing the pinch-off of double emulsion droplets in narrowing jetting regime are shown in Figs. 7 and 8. The transition from dripping to narrowing jetting was achieved by an increase in Q_3 from 2.47 to 24 ml/h while keeping all other parameters constant. The total droplet formation time is $\tau_2 = 154$ and the inner droplet pinches off at $\tau_1 = 86$. The necking starts with elongation and localised narrowing of a compound jet, which leads to the formation of a high pressure region in the neck and ultimate breakup of the compound thread. Two main differences between dripping and narrowing jetting regime are: (i) the pressure in the middle of the neck at the moment of pinch-off is considerably lower in narrowing jetting than that in dripping regime which is a consequence of a higher velocity in the neck; (ii) a vortex flow does not arise in the narrowing jetting and the jet breakup occurs due to high velocity in the thread at its downstream end (Fig. 8d). A reason for different behaviour is that the viscous force exerted on the thread by the outer fluid is much higher in the narrowing jetting than in dripping regime. As can be seen in Table 2, Capillary number of the outer fluid in the necking region, $Ca_3 = \mu_3 V_3/\sigma_{23}$ (where σ_{23} is the interfacial tension between phase 2 and phase 3, μ_3 is the dynamic viscosity of outer phase, and V_3 is the velocity at the outer interface of the neck), which represents the relative effect of viscous forces versus surface tension acting across the outer interface, is 4–9 times higher in the dripping than narrowing jetting. The satellite formation was also observed as a result of fragmentation of the threads of inner and outer fluid. However, in the case of inner fluid, due to high velocity at the downstream end of the thread, the inner fluid rapidly
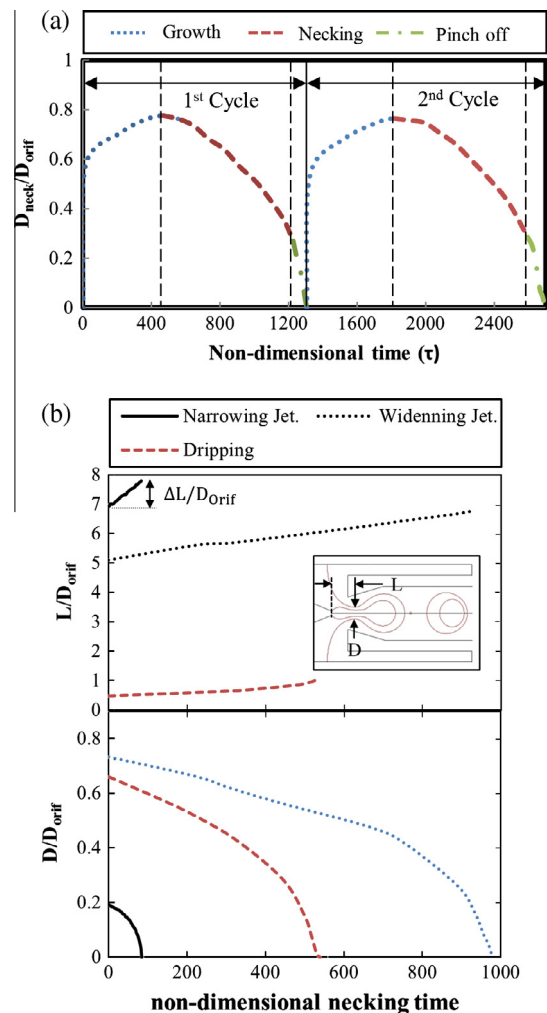

Fig. 9. (a) A neck diameter of a compound jet as a function of non-dimensional time during droplet formation in dripping regime; (b) the evolution of compound jet shape with non-dimensional time during necking in different regimes: (top) the axial distance of the neck from the injection nozzle, L; (bottom) the neck diameter, D_{neck}. The conditions in different regimes are specified in Figs. 3, 5 and 6.

retracts towards the primary inner droplet which prevents the thread pinch-off and formation of core satellite droplets inside the primary double emulsion droplet (Fig. 8d).

4.4. Characterisation of pinch-off process

A periodic variation of D_{neck} as a function of non-dimensional time for droplet formation in the dripping regime over two consecutive cycles is shown in Fig. 9a. The droplet formation pattern in both cycles is similar reflecting the fact that droplets produced by dripping are uniform in size, with a coefficient of variation typically less than 3%. Droplet generation can be divided into three successive steps: droplet growth (τ = 0–465), necking (τ = 465–1225), and pinch-off (τ = 1225–1324). Droplet growing begins with retrieving the remaining thread which connected the detached double emulsion droplet to the compound jet, and continues with enlarging the subsequent double emulsion droplet. As the size of the double emulsion droplet grows, the drag force exerted by the outer fluid increases. The necking begins once the drag force (which tends to stretch the droplet downstream) becomes comparable with the interfacial tension force tending to pull back the forming droplet towards the injection nozzle. The pinch-off step is characterised by a fast reduction in the compound jet diameter, which eventually results in droplet detachment.

The variation of D_{neck}/D_{Orif} and L/D_{Orif} with τ for droplet breakup in different regimes is shown in Fig. 9b, where D_{neck} is the diameter of the narrowest constriction of the jet and L is its downstream distance from the injection nozzle. Zero time (τ = 0) corresponds to the onset of necking, when the coaxial jet begins to narrow. The necking begins with a very moderate reduction in D_{neck}, which is followed by a steep decrease of D_{neck} down to zero in the final stage of pinch-off (Fig. 9b). In narrowing jetting regime, jet pinch-off occurs rapidly and the jet at the onset of necking is very narrow with $D_{neck}/D_{Orif} \approx 0.2$. In narrowing jetting, the necking starts at $L = 6.6D_{Orif}$ and the breakup occurs at $L = 7.7D_{Orif}$. In widening jetting, the necking starts at $L = 4D_{Orif}$ and the breakup occurs at $L = 6.7D_{Orif}$. In dripping regime, the necking and pinch-off occurs within one orifice diameter downstream of the orifice. A novel equation for the shear stress at the outer interface, $\sigma_{2,3}$ has been developed, as follows:

$$\sigma_{2,3} = \frac{32\mu_3 Q_3}{\pi} \frac{\alpha}{D_{orif}^3(\alpha^2 - 1)^2} \tag{9}$$

where $\alpha = D_{jet}/D_{Orif}$. At the start of necking, $\sigma_{2,3} \approx 25$ Pa and then decreases with time until it reaches zero. Since $\sigma_{2,3}$ decreases as the neck is thinning, the shear stress exerted by the outer phase is not a reason for pinch-off. However, the Laplace pressure is inversely proportional to the compound jet diameter, $\Delta P = 2\gamma/D$; therefore a reduction in D_{neck} increases the Laplace pressure and thus accelerates the necking, which ultimately leads to pinch-off.

In widening jetting regime, the jet breakup is caused by the high velocity gradient across the outer interface leading to dissipation of the jet momentum by the outer phase. The final stage of the necking begins at $\tau \approx 1600$ (Fig. 9b) when the Weber number of the compound jet, We_2, is 0.002, where $We_2 = \rho_2 V_2^2 D_{neck}/\sigma_{23}$ and V_2 is the average velocity of the compound jet in the neck. The formation of vortex flow results in a noticeable reduction of We_2, which results in strengthening of the vortices and further dissipation of the jet momentum until the neck finally pinches off.

In Fig. 9b, the slope of the L/D_{Orif} versus τ lines, $[D_{Orif}^{-1}(\partial L/\partial \tau)]$, is proportional to the speed at which the neck of the compound jet moves downstream before it pinches off. The neck moves at the maximum speed in the narrowing jetting regime, followed by widening jetting and dripping regime respectively. It can be attributed to the highest shear at the outer surface of the thread in the narrowing jetting, as can be seen from Ca_3 values in Table 2. In widening jetting regime, the neck of the thread travels the longest distance ΔL before it collapses.

5. Conclusions

In this study, a novel VOF–CSF numerical model was developed to investigate the break-up mechanisms of double emulsion within a three-phase glass capillary device for the dripping, widening jetting, and narrowing jetting regimes. Formation of compound drops in microfluidic devices was simulated by Vu et al. [24] for co-flowing streams and Zhou et al. [22] for co-flow focusing geometry, but the device modelled in this work is more complex and combines simple co-flow geometry and counter-current flow focusing [15]. The droplet formation in different regimes was found to be dominated by different phenomena and distinct forces, which leads to non-identical droplet break-up mechanisms. It emphasises the necessity of including all regimes of drop generation into consideration, rather than dealing just with the dripping regime [24]. The model was validated experimentally and a good agreement between simulations and experiments was obtained. The model was capable of accurately reproducing the droplet formation in all reported regimes [15] including satellite and sub-satellite formations. In addition, the model allows for all three fluid streams to have different physical properties, which enables more realistic simulations, compared to the previous model [22] where inner and outer fluid had the same properties. Based on simulated pressure distributions and velocity fields, it was found that the jet pinch-off in dripping and widening jetting was accompanied by formation of vortex flows around the upstream end of the necking thread. Due to the presence of vortex flow, the thread remainders were retracted in both regimes, but it was more pronounced in dripping mode. In widening jetting regime, the pinch-off of the outer interface was caused by the high velocity gradient at the interface, leading to a dramatic dissipation of a compound jet momentum. In the narrowing jetting regime, no vortex flow was observed and the droplet pinch-off occurred due to higher velocity at the downstream end of the thread compared to that at the upstream end. In all regimes, the inner jet ruptures before the outer jet, which prevents a leakage of the content of an inner drop into the outer fluid and ensures high encapsulation efficiency. The speed at which the neck of a double jet moves downstream was proportional to the Capillary number of the outer fluid, with the highest speed observed in the narrowing jetting and the slowest speed in dripping regime. In widening jetting, the coaxial neck travels the longest distance before it breaks.

This study may advance the current understanding of compound thread break-up in microfluidic devices by indicating the exact flow vector and pressure distributions around the interfaces and highlighting the distinct nature of the jet pinch-off in different regimes. It can help to achieve an active control over the pinch-off process of compound jets in microfluidic devices and limit formation of satellite droplets. By implementing the effect of surfactant in the present model, it will be possible to model formation of compound droplets containing a controlled number of inner droplets within each outer drop [40] and improve the understanding of multi-cored double emulsion formation.

Appendix A. Supplementary material

Supplementary data associated with this article can be found, in the online version, at http://dx.doi.org/10.1016/j.jcis.2015.03.032.

References

[1] R. Arshady, Microspheres Microcapsules and Liposomes: Preparation and Chemical Applications, Citus Books, London, 1999.
[2] G. Muschiolik, Curr. Opin. Colloid Interface Sci. 12 (2007) 213.
[3] C. Laugel, A. Baillet, M.P. Youenang Piemi, J. Marty, D. Ferrier, Int. J. Pharm. 160 (1998) 109.
[4] M.H. Lee, S.G. Oh, S.K. Moon, S.Y. Bae, J. Colloid Interface Sci. 240 (2001) 83.
[5] C.J. Martinez, J.W. Kim, C. Ye, I. Ortiz, A.C. Rowat, M. Marquez, D. Weitz, Macromol. Biosci. 12 (2012) 946.
[6] R.D. Aines, C.M. Spaddaccini, E.B. Duoss, K. Joshuah, J. Vericella, J.A. Lewis, G. Farthing, Energy Procedia. 37 (2013) 219.
[7] K. Nakagawa, S. Iwamoto, M. Nakajima, A. Shono, K. Satoh, J. Colloid Interface Sci. 278 (2004) 198.
[8] J.H. Han, B.M. Koo, J.W. Kim, K.D. Suh, Chem. Commun. 28 (2008) 984.
[9] E. Donath, G.B. Sukhorukov, F. Caruso, S.A. Davis, H. Möhwald, Angew. Chem. Int. Ed. (1998) 2201.
[10] P.J. Dowding, R. Atkin, B. Vincent, P. Bouillot, Langmuir 20 (2004) 11374.
[11] E. Mathiowitz, H. Bernstein, S. Giannos, P. Dor, T. Turek, R. Langer, J. Appl. Polym. Sci. 45 (1992) 125.
[12] N. Pannacci, H. Bruus, D. Bartolo, I. Etchart, T. Lockhart, Y. Hennequin, H. Willaime, P. Tabeling, Phys. Rev. Lett. 101 (2008) 164502.
[13] T. Nisisako, S. Okushima, T. Torii, Soft Matter 1 (2005) 23.
[14] C. Cramer, P. Fischer, E.J. Windhab, Chem. Eng. Sci. 59 (2004) 3045.
[15] A.S. Utada, E. Lorenceau, D.R. Link, P.D. Kaplan, H.A. Stone, D.A. Weitz, Science 308 (2005) 537.
[16] G.T. Vladisavljević, H. Shahmohamadi, D.B. Das, E.E. Ekanem, Z. Tauanov, L. Sharma, J. Colloid Interface Sci. 418 (2014) 163.
[17] T.P. Lagus, J.F. Edd, J. Phys. D: Appl. Phys. 46 (2013) 114005.
[18] P.W. Chen, R.M. Erb, A.R. Studart, Langmuir 28 (2012) 144.
[19] F.C. Chang, Y.C. Su, J. Micromech. Microeng. 18 (2008) 065018.
[20] Z. Chang, C.A. Serra, M. Bouquey, L. Prat, G. Hadziioannou, Lab Chip 9 (2009) 3007.
[21] L. Chu, A.S. Utada, R.K. Shah, J. Kim, D.A. Weitz, Angew. Chem. Int. Ed. 46 (2007) 8970.
[22] C. Zhou, P. Yue, J.J. Feng, Phys. Fluids 18 (2006) 092105.
[23] J.M. Park, P.D. Anderson, Lab Chip 12 (2012) 2672.
[24] T.V. Vu, S. Homma, G. Tryggvason, J.C. Wells, H. Takakura, Int. J. Multiph. Flow 49 (2013) 58.
[25] R.M. Erb, D. Obrist, P.W. Chen, J. Studer, A.R. Studart, Soft Matter 7 (2011) 8757.
[26] G.T. Vladisavljević, H.C. Shum, D.A. Weitz, Prog. Colloid Polym. Sci. 139 (2012) 115.
[27] J.G. Santiago, S.T. Wereley, C.D. Meinhart, D.J. Beebe, R.J. Adrian, Exp. Fluids 25 (1998) 316.
[28] R. Lindken, M. Rossi, S. Grosse, J. Westerweel, Lab Chip 9 (2009) 2551.
[29] M. Tjahjadi, H.A. Stone, J.M. Ottino, J. Fluid Mech. 243 (1992) 297.
[30] Y. Chen, L. Wu, C. Zhang, Phys. Rev. E 87 (2013) 013002.
[31] H.A. Stone, L.G. Leal, J. Fluid Mech. 211 (1990) 123.
[32] S. Radev, B. Tchavdarov, Int. J. Multiph. Flow 14 (1988) 67.
[33] A. Chauhan, C. Maldarelli, D.T. Papageorgiou, D.S. Rumschitzki, J. Fluid Mech. 420 (2000) 1.
[34] R. Suryo, P. Doshi, O.A. Basaran, Phys. Fluids 18 (2006) 082107.
[35] X. Zhang, Chem. Eng. Sci. 54 (1999) 1759.
[36] Y. Chen, X. Liu, M. Shi, Appl. Phys. Lett. 102 (2013) 051609.
[37] Y. Ren, Z. Liu, H.C. Shum, Lab Chip (2014).
[38] C. Hirt, B. Nichols, J. Comput. Phys. 39 (1981) 201.
[39] J. Brackbill, D. Kothe, C. Zemach, J. Comput. Phys. 100 (1992) 335.
[40] D. Lee, D.A. Weitz, Small 5 (2009) 1932.